Productivity evaluation of hydraulically fractured gas-condensate reservoirs

Shi-Yi Zheng[1], Murat Zhiyenkulov[2] and TongChun Yi[3]
[1] *Institute of Petroleum Engineering, Heriot-Watt University, Edinburgh EH14 4AS, UK*
(e-mail: shiyi.zheng@pet.hw.ac uk)
[2] *Schlumberger, Karzastan*
[3] *Schlumberger, Geoquest UK*

ABSTRACT: This study describes an application of a compositional single well simulator to analyse well tests in gas-condensate reservoirs. An important aspect of this application for gas-condensate well tests is accurate fluid property prediction during the multi-phase flow regime, which occurs in the near-well region. The simulator can also be used to understand the impact of liquid drop-out and fracture flow on well productivity.

Hydraulic fracturing improves the economics of wells drilled in tight reservoirs. However, the operation involves a significant amount of expenditure. In recent years this technique has also been used to stimulate gas-condensate reservoirs by creating a flow conduit through the condensate banking near the well. Thus, it is crucial to keep a fracture as small as possible. In practice it has been proved that a short, wide fracture can provide much higher production than the traditionally pursued narrow, long fracture.

The workflow in this study contains compositional simulation of a single well in a tight gas-condensate reservoir, which is used to generate transient pressure data for well test analysis and interpretation to predict multi-phase flow behaviour, and to analyse productivity impairment due to condensation. Simulation models were then further modified to study the impact of various hydraulic fractures on the well productivity index (PI), which is defined as the ratio of production rate (constant) divided by the pressure drop across the reservoir. PIs for fractured cases are compared with respect to the non-fractured base case. Streamline simulation of the fractured gas-condensate reservoir was also included in the study to allow visualization of the flow profile in and around the hydraulic fracture.

KEYWORDS: *condensate banking, hydraulic fracturing, multi-phase flow, compositional model, pseudo pressure*

INTRODUCTION

When a gas reservoir produces liquid (condensate) together with the gas, it is called a wet gas or gas-condensate reservoir. Figure 1 shows a phase diagram for the classification of various reservoirs with respect to their initial reservoir pressure and temperature. The difference between gas-condensate and wet gas is their condensate-gas ratio (CGR). According to reservoir engineering studies, for a dry gas reservoir, the CGR is less than 10 (BBL/$\times 10^6$ SCF) while, for a wet gas reservoir the CGR is about 10–30 (BBL/$\times 10^6$ SCF). When the CGR is greater than 50 (up to 300 BBL/$\times 10^6$ SCF), the reservoir is defined as a rich gas-condensate reservoir. Sometimes engineers will also refer to a lean gas (condensate) reservoir, where the CGR falls between those of wet gas and gas-condensate reservoirs. A strict definition of the above reservoirs should be made through the corresponding phase diagram, which is beyond the scope of the current paper. During the production of a gas-condensate reservoir, the liquid phase condenses initially during isothermal depletion and then re-vaporizes as pressure depletion continues (Towler 1999). When a well produces at a bottom-hole pressure lower than the dew point pressure, retrograde condensation starts and forms condensate bank around the well. The near-well area can be divided into three zones with respect to fluid flow conditions in the reservoir (Fig. 2). In zone 1, closest to the well, the amount of condensate drop-out exceeds critical saturation and, therefore, two-phase flow occurs. In zone 2, however, the condensate amount is below critical saturation, thus only gas flows. Permeability to gas in these zones is reduced by the presence of a second phase. In zone 3, there is only a gas phase as the reservoir pressure is above the dew point pressure in this zone.

Traditional single-phase dry gas well test interpretation fails in the presence of this second mobile phase. Jones & Raghavan (1988) proved failure of applying the single-phase dry gas analysis method to gas-condensate reservoirs and proposed a method of computing multi-phase pseudo pressure (MPPP) using fluid properties (density and viscosity) and relative per-

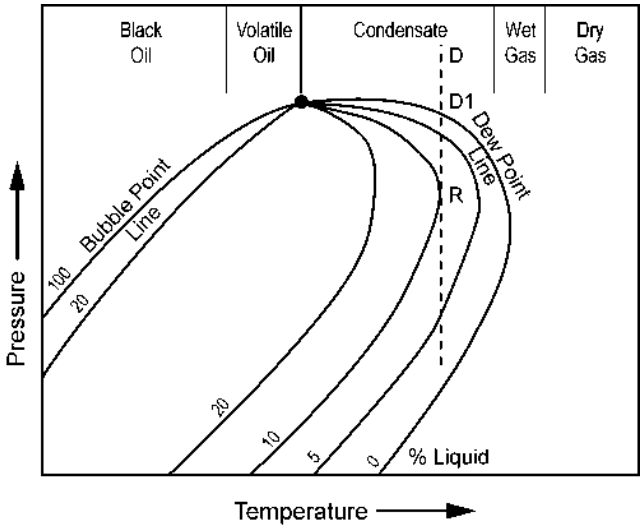

Fig. 1. Phase diagram for classifying various types of reservoirs.

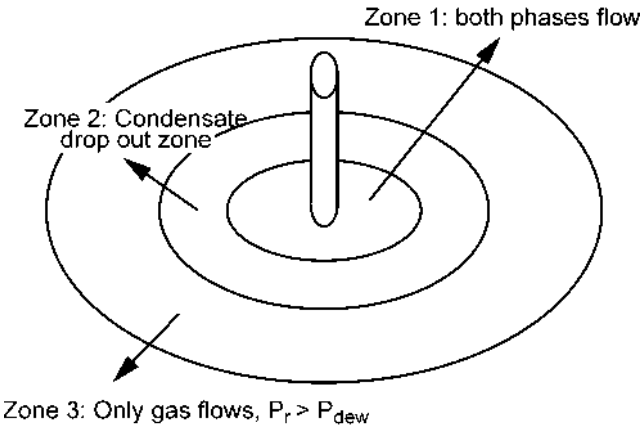

Fig. 2. Three zones around a gas-condensate well producing at $P_{bh} < P_{dew}$.

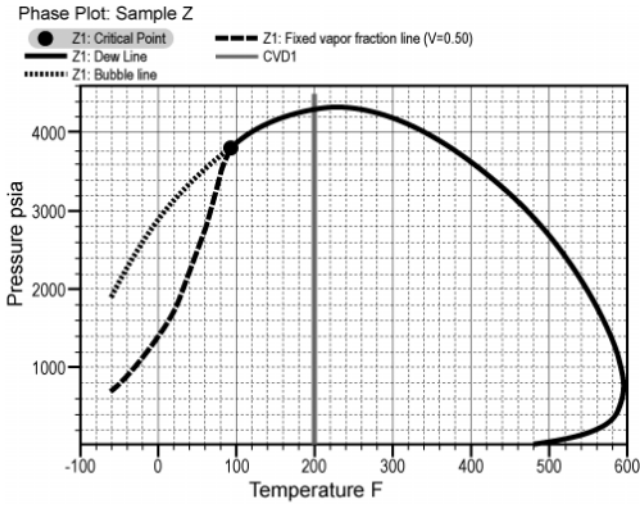

Fig. 3. Phase diagram of the fluid used for well test simulation studies.

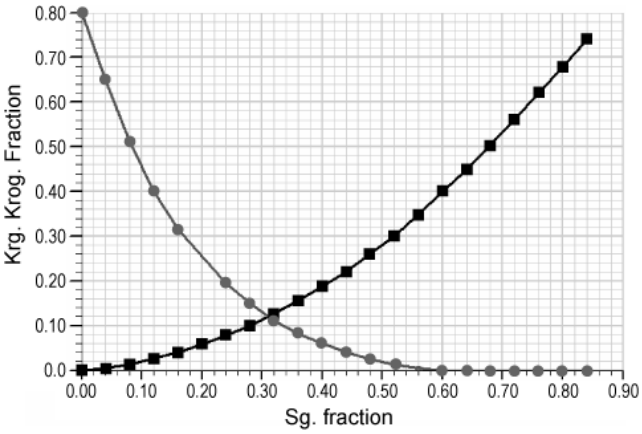

Fig. 4. Oil and gas relative permeability curves used in the study.

meability curves of both phases. Blom & Hagoort (1998) showed that well productivity is reduced severely due to liquid drop-out in the near-well zone. They also investigated capillary number-dependent relative permeability and non-Darcy flow impact on the well productivity. Studies conducted by Carlson & Myer (1995) and Settari *et al.* (1996) showed that hydraulic fracturing is an effective method to remedy the condensate bank around the well. Carlson & Myer's (1995) work included comparison of productivities after acid and fracture procedures and liquid drop-out impact on the fractured well. Rae *et al.* (1999) showed that, in low permeability reservoirs, a significant improvement in productivity index (PI) could be obtained from a small hydraulic fracture. They investigated how parameters, such as well skin, fracture height, fracture length and conductivity, influence the PI. Their work, however, was limited to gas and oil reservoirs. Bertram *et al.* (1997) and Yadavalli & Jones (1996) showed a numerical approach to well testing in non-fractured and fractured gas-condensate reservoirs. However, Bertram *et al.*'s (1997) work did not include interpretation of well test data. They compared their simulation results with measured datasets. Saleh (1992) presented a dimensionless form of Jones & Raghavan's (1988) MPPP computation method, and this method is implemented in PanSystem (EPS product).

The objective of this study is to document all the issues discussed by the different authors mentioned above. Numerical well testing studies are then conducted on this basis in order to prove that in tight gas-condensate reservoirs, higher productivity can be obtained from a short and wide fracture created from hydraulic fracturing. The parameters investigated in the study are fracture half-length and width. The result of the study also proved that the short, wide fracture, which can be achieved from the current industry fracturing technique, is sufficient to bypass the liquid drop-out zone (condensate banking), leading to an increase in well productivity.

SIMULATION MODEL DESCRIPTION

A 3D radial compositional model with AdapTable IMplicit option (AIM) using the modified Peng–Robinson cubic equation of state (EOS) was used to generate pressure transient data. Schlumberger provided the relative permeability and PVT data required for the study. The study was based on a nine-component fluid description from PVT testing. The phase diagram of the fluid is shown in Figure 3. One set of relative permeability curves for gas and oil (shown in Fig. 4) is used in the study. The rate dependency of relative permeability curves is not considered in the simulations. The base model has a radius of 2615 ft, which is larger than the radius of the investigation of the well test during the pressure drawdown and build-up, in order to ensure a clear infinite acting pressure response at the outer boundary. The model has five layers to study the gravity effect on the condensation during production.

Table 1. *Reservoir parameters*

Parameters	Values
Permeability (mD)	1
Porosity (%)	10
Reservoir thickness (ft)	100
Initial pressure (psi)	4356
Dew point pressure (psi)	4298
Reservoir temperature (°F)	200
Condensate-gas ratio (STB/ × 10^6 SCF)	86.75
Oil gravity (API)	57.17

Table 2. *Fluid composition*

Component name	Mole fraction	Mole weight (lb/lb.mole)
CO_2	0.0121	44.01
N_2	0.0194	28.013
C_1	0.6599	16.043
C_2	0.0869	30.07
C_3	0.0591	44.097
C_{4-6}	0.0967	66.869
C_{7+1}	0.04745	107.78
C_{7+2}	0.01515	198.56
C_{7+3}	0.0033	335.2
Total	1	

Reservoir data (properties) and fluid composition are given in the Tables 1 and 2, respectively.

Time step sensitivity for well test simulations was not performed. Instead a well test with the same flow rate history, reservoir size (thickness and area) and description (permeability and porosity) was simulated using Weltest 200^{TR} and its TUNING and TSTEP keywords are used in all simulations. A sensitivity study on radial grid size was performed by using two other models. First, with finer grids and, the second, with coarser grids. Three models were evaluated by using dry gas PVT data for simulation grid effects. Using analytical methods, the well test pressure responses generated from the models were analysed. A good match between simulation input parameters and PanSystem output results was obtained for the current and fine grid models. Due to the time limit, the finer model was not used for the study. Additionally, the current model was tested for two different reservoir permeabilities, 1 mD and 100 mD, using the same dry gas PVT data. A consistent result between permeability values estimated from dry gas well test interpretation and simulation input values was obtained.

WELL TEST SIMULATION

A multiple-rate flow-after-flow test was simulated using the simulation model as shown in Figure 5. The test consisted of four pressure drawdowns and a final build-up: the first three drawdowns were 0.333 days long (8 hr) each at an increasing rate of 200×10^3, 400×10^3 and 800×10^3 SCF per day (SCFD); the last draw down was 2.766 days at a rate of 1600×10^3 SCFD and the final build-up lasted for 11 days. The reservoir pressure was above the dew point pressure, P_{dew}, initially, but fell below it in the near-well region during the test. The radius of investigation of the simulated well test was predicted from equation (1):

$$R_{inv} = 0.03\sqrt{\frac{kt_p}{\varphi \mu C t}} \quad (1)$$

Although the simulation model has a radius of 2615 ft, which is larger than the pressure transient reaches during the well test, pressure versus time plots (Cartesian plots) from all drawdown periods show a depleting reservoir response (i.e. pressure continuously falls during the drawdown; it does not stabilize, as shown in Fig. 5). This response becomes more obvious at higher production rates. A simulation with a flowing period of one month for the last drawdown was performed during the study. However, the pressure did not stabilize either at the end of the drawdown, thus it was decided to keep to short flow period due to time limits in this study.

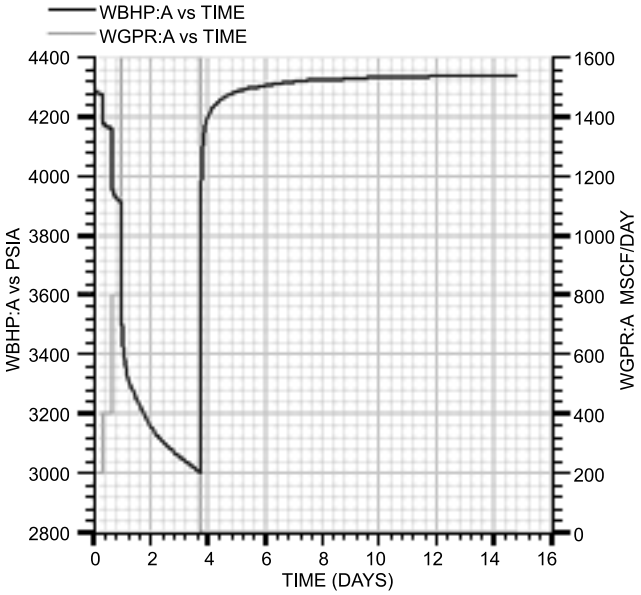

Fig. 5. Well bottom-hole pressure and flow rates change with time during the well test simulation.

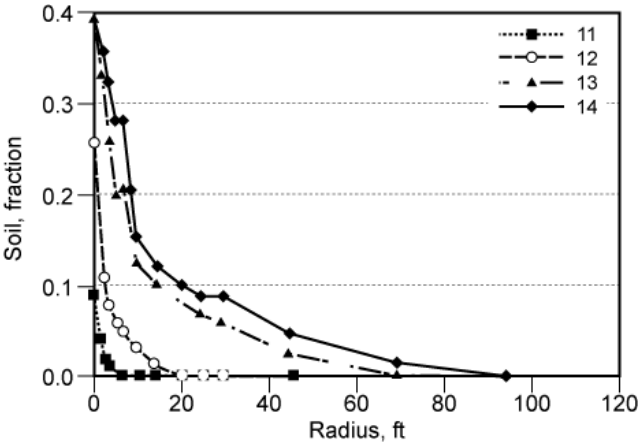

Fig. 6. Liquid drop-out radius changes during pressure drawdown periods (from base case model).

The base simulation model, used for well test and pre-fracture simulations, does not include the effects of non-Darcy flow and rate dependency of relative permeability curves. A study conducted by Blom & Hagoort (1998) showed that the non-Darcy flow effect is more pronounced in gas-condensate reservoirs compared to dry gas reservoirs. They concluded that liquid drop-out and, consequently, well productivity impairment can be overestimated if the non-Darcy flow effect is ignored.

Figures 6 and 7 show the propagation of a condensate bank around the wellbore during drawdown periods from the base model and the model which considers the non-Darcy flow

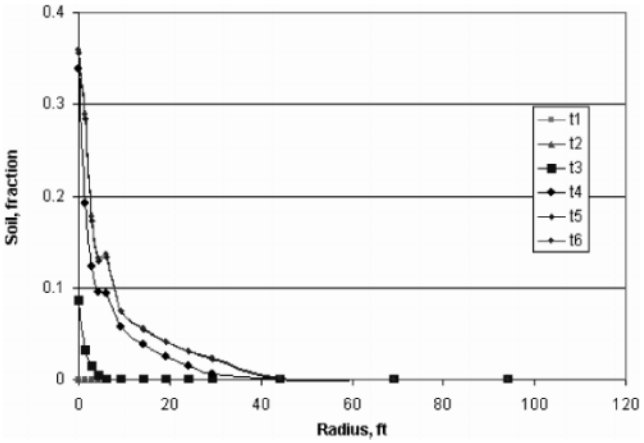

Fig. 7. Liquid drop-out radius changes during drawdown periods (model including non-Darcy flow effect).

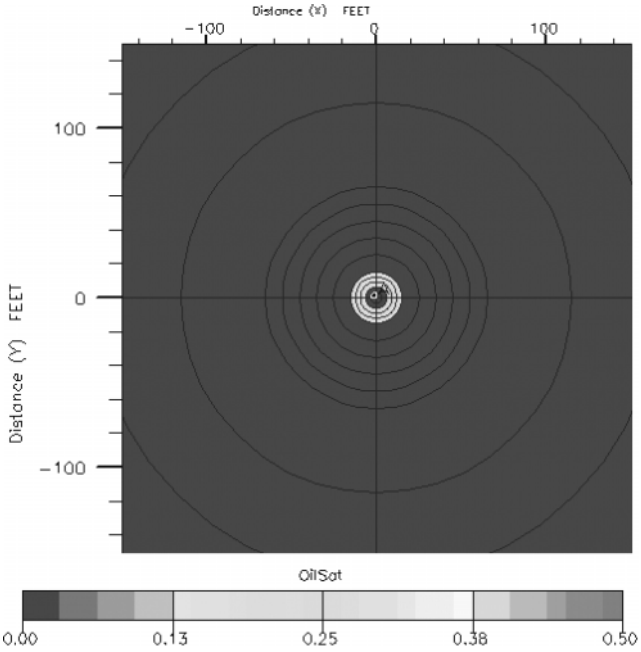

Fig. 8. Liquid saturation at the end of pressure build-up.

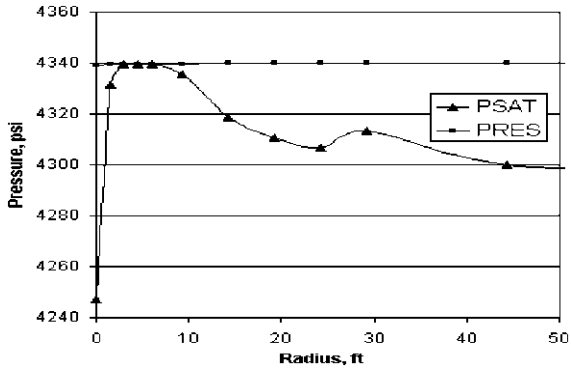

Fig. 9. Saturation and reservoir pressures at the end of pressure build-up.

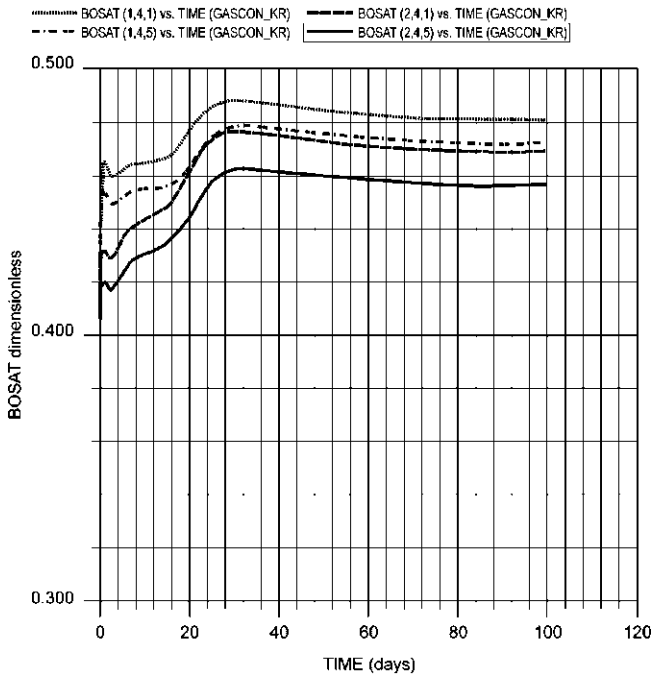

Fig. 10. Liquid saturation around the well after a long production period.

effect. The liquid drop-out radius increases with increasing drawdown pressure in both cases. Comparison of results from two simulations verifies that it appears to have less liquid drop-outs in the presence of non-Darcy flow in the reservoir.

The simulations also showed that once liquid drops out, its re-vaporization takes a long time. The simulation results in Figure 8 show liquid saturation around the well (a radius between 6 ft and 15 ft) at the end of the 11-day build-up. It can be seen that there is still a significant amount of liquid near the well, despite reservoir pressure being higher than or equal to saturation pressure at the end of the build-up, as shown in Figure 9. The variation in the saturation pressure with respect to radius is due to a change in fluid property from its initial state in the near-well zone. This was caused by condensation of heavy components during the drawdown periods.

CONDENSATE BANK STABILIZATION

The condensate bank radius observed during well test drawdown periods was short (a few feet) and not fully stabilized. Analysis of transient pressures generated by the simulation confirmed propagation of condensate banking during drawdowns. Thus, a long period of production controlled by bottom-hole pressure was simulated to determine the time required for the condensate bank to stabilize. The results of the simulation are presented in Figures 10 and 11, respectively.

Figure 10 shows the liquid saturation changing together with the production time near the well. Liquid saturation stabilizes at 48% for the block (1, 4, 1). This is after only about 80 days of production. Figure 11 shows the gas: oil ratio (GOR) (top dots), gas rate (middle dashes) and oil rate (bottom solid line) during the long production time simulation. They also stabilized at about 80 days. Stabilization of oil saturation and GOR in the near-well zone is an indication that a condensate bank has formed and stabilized.

As this study focuses on the well testing aspect of gas-condensate reservoirs and 80 days of production is not practically viable, it was decided to keep flow rate settings as discussed in the previous section. Clearly, a long production period required for the formation of a stable condensate bank can be another study topic for tight gas-condensate reservoirs.

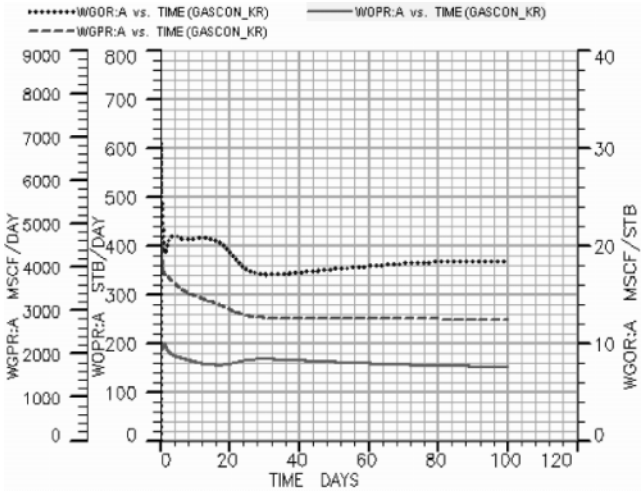

Fig. 11. GOR (top dots), gas rate (middle dashes) and oil rate (bottom solid line) changes with time.

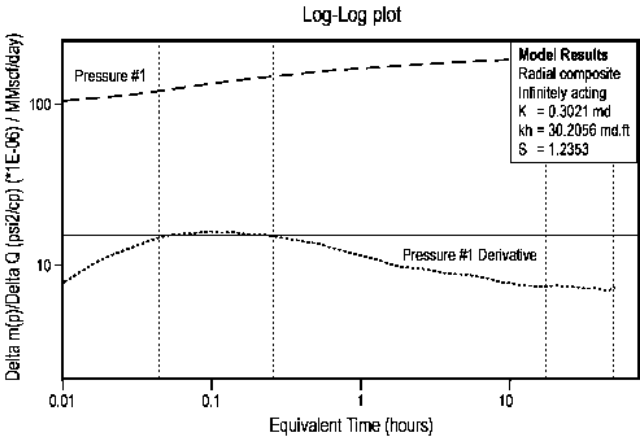

Fig. 12. Log–log plot of a simulated multi-phase flow well test analysis using the dry gas pseudo pressure method.

WELL TEST ANALYSIS AND INTERPRETATION

Pressure responses from the gas-condensate well generated by the simulation model were analysed using two methods: (1) single-phase dry gas pseudo pressure; and (2) multi-phase pseudo pressure.

Analysis using single-phase pseudo pressure

The transient pressure data from the gas-condensate well test were interpreted initially using a conventional dry gas pseudo pressure, computed using equation (2):

$$m(P) = 2\sum_{P_{wf}}^{P} \frac{P}{\mu z} dP \qquad (2)$$

Log–log and semi-log plots, together with the results using the dry gas pseudo pressure method, are shown in Figures 12 and 13, respectively. A typical radial composite effect due to liquid drop-out is observed on the log–log plot of the simulated data. The true skin and non-Darcy flow coefficient of 0 is used in the simulations. The well penetrates the reservoir zone fully (i.e. no partial penetration effect), thus skin values estimated from well test interpretation are purely due to liquid drop-out. The analysis shows that permeability in the single-phase outer zone

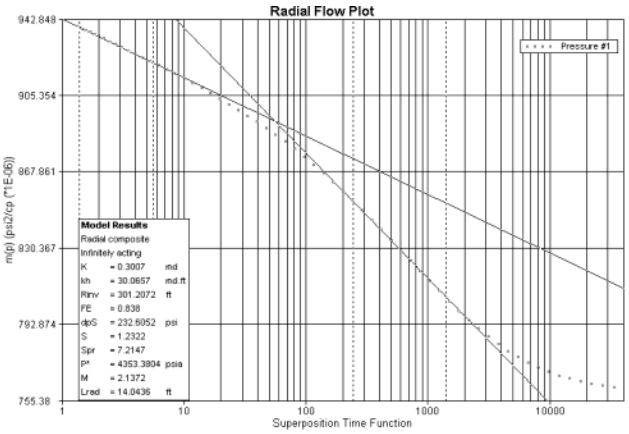

Fig. 13. Semi-log plot of a simulated multi-phase flow well test analysis using the dry gas pseudo pressure method.

is, k_{out}=0.65 mD, which is lower than the expected value of 0.74 mD. (The effective permeability, k_{effg}, in a single-phase gas region is 0.74 mD, which is calculated from $k_{effg}=k_{abs} \times k_{rg}$ @ S_{wc}, $k_{effg}=1 \times 0.74=0.74$ mD.) The ratio of outer zone permeability to inner zone permeability is $k_{out}/k_{in}=0.65/0.30=2.2$.

Analysis using multi-phase pseudo pressure

This method requires the calculation of multi-phase (or two-phase) pseudo pressure (MPPP) and importing the data into a relevant well testing package for the analysis. In this study, the MPPP is calculated using equation (3) and then the results are imported into Pansystem (Saleh 1992).

$$\psi(P) = \frac{\mu_i}{\rho_i}\sum_{Pwf}^{P}\left(\frac{k_{ro}\rho_o}{\mu_o} + \frac{k_{rg}\rho_g}{\mu_g}\right)dP \qquad (3)$$

Two approaches are attempted in MPPP computation: the first method uses condensate fluid properties obtained from the simulated constant volume depletion (CVD) experiment, while the second uses fluid properties exported from the simulation model. The limitation of calculations based on the CVD experiment is that the amount of maximum liquid drop-out observed during the CVD does not exceed 23%. However, the simulation shows that liquid saturation near the well region exceeds that value and can reach up to 40%. Thus k_{rg} and k_{ro} values predicted by the two approaches should be different. MPPP versus normal pressure plots from both methods is shown in Figures 14 and 15, respectively.

In the first method, condensate and gas density and viscosity were obtained by simulating a CVD experiment using the PVTi package. Then the ratio of k_{rg}/k_{ro} at each pressure level was calculated from equation (4) (Jones & Raghavan 1988; Saleh 1992).

$$\frac{k_{ro}}{k_{rg}}(S_g) = \frac{L\rho_g\mu_o}{V\rho_o\mu_g} \qquad (4)$$

Where L and V are liquid and gas saturations at equilibrium estimated from the CVD experiment, ρ and μ are liquid and gas density and viscosity. Then the gas saturation values were interpolated from the k_{rg}/k_{ro} versus S_g plot. The individual relative permeability values were estimated using the gas saturation predicted in the previous step. The computed MPPP table was then imported into PanSystem.

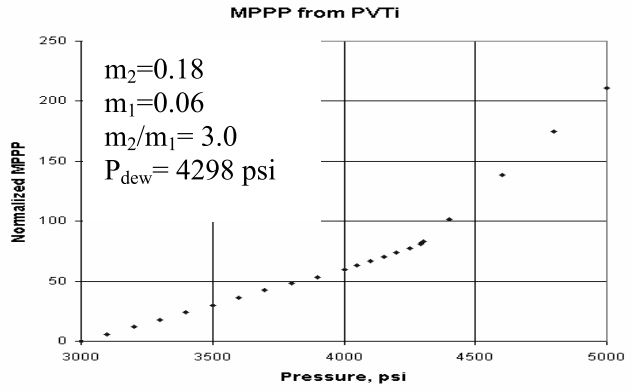

Fig. 14. MPPP computation using fluid properties predicted from the CVD experiment.

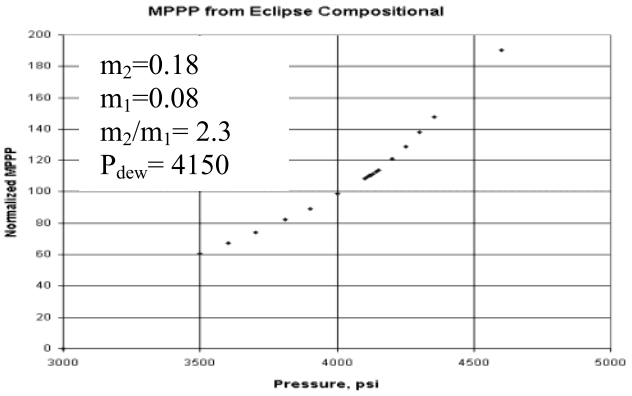

Fig. 15. MPPP computation using fluid properties derived from the simulation.

In the second method, all input parameters for equation (3) were exported directly from the simulation model for block (1, 4, 1). Then the MPPP pressure was computed using an Excel[TR] spreadsheet.

The MPPP plot for the first method shows P_{dew}=4298 psi. However, the ratio of slopes m_2/m_1=3.0, which is higher than the ratio of k_{out}/k_{in}. This was calculated in the previous section. Output from the simulation takes into account an increase in oil saturation above 23% and calculates relative permeabilities accurately. A P_{dew}=2150 psi is obtained from the second method, which is lower than the original P_{dew}. But the ratio of m_2/m_1=2.3 is very close to the ratio of k_{out}/k_{in}=2.2.

Figures 16 and 17 show well test analysis results using MPPP computed by both methods respectively. Although both methods show similar permeability values, they are slightly overestimated. However, the skin value estimated by the first method is negative and far from reality. Similar fluid properties were estimated at the same pressure level by both methods. However, relative permeability values were significantly different due to the difference in liquid saturations observed in the study. The difference and strange shape of the pressure derivative curve from the first method is caused possibly by wrongly estimated relative permeability data in the two-phase flow region. Permeability is overestimated by a factor of two when the lower horizontal section of the derivative is used for radial flow analysis.

HYDRAULIC FRACTURE MODEL DESCRIPTION

The reservoir area used in the fracturing simulations is 5000 ft by 5000 ft. Proppant was pumped into the fracture, with a

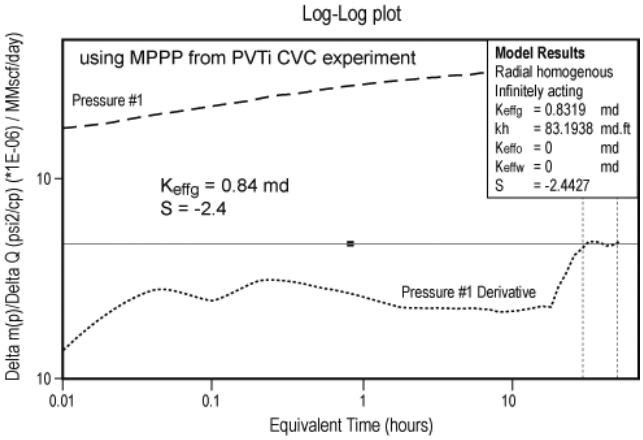

Fig. 16. Log–log plot using MPPP computed from fluid properties predicted from the CVD experiment.

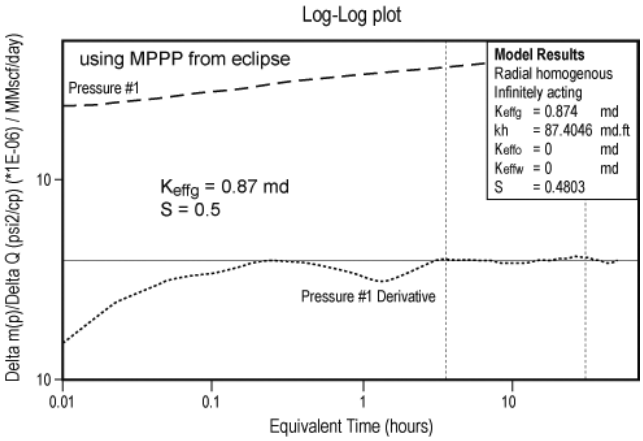

Fig. 17. Log–log plot using MPPP computed from fluid properties derived from the simulation.

permeability and porosity of 273 D and 0.35, respectively, typical for 20/40 mesh Colorado Sand. Gas and condensate relative permeability curves in the fracture are assumed to have straight-line characteristics. The relative permeability for one phase is zero at zero saturation of that phase and 1 when the saturation is 1 (i.e. k_{rg}=0 at S_g=0 and k_{rg}=1 at S_g=1; it is the same for the liquid phase). Fracture lengths and widths are selected to cover different ranges in practice. Fractures are assumed to cover full reservoir zone thickness.

Grid sizes increase in the directions both along and perpendicular to a hydraulic fracture. Finer grids are built at the fracture tips in order to capture the flow convergence during flow. The hydraulic fracture is assumed to have a constant width and height from the wellbore to the tip. A typical grid structure is shown in Figure 18.

WELL PI BEFORE AND AFTER FRACTURING

One of the objectives of this study is to determine the impact of various fracture geometries on improvement of well PI. Figure 19 shows an initial pre-fracture case, which is used as the base case to compare the efficiency of different hydraulic fractures. (Note: this simulation has a shorter drawdown period (and smaller flow rates) than the one used for well test interpretation. In the well test simulation, the last drawdown period is extended and flow rates are doubled to magnify the two-phase flow impact on pressure data.) Initially, the well PI remains constant at 7.5×10^3 SCFD/STB; however, as pressure

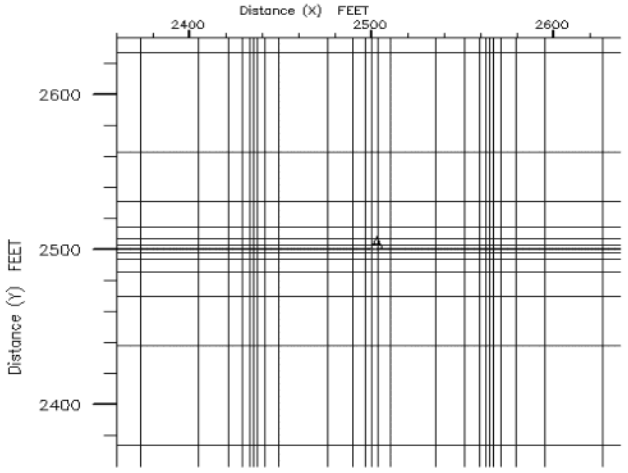

Fig. 18. Fracture grids, zoomed view.

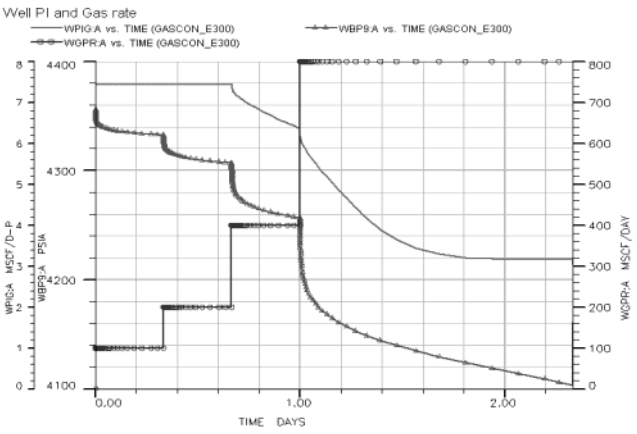

Fig. 19. Well PI, BHP and gas rate versus time before fracturing.

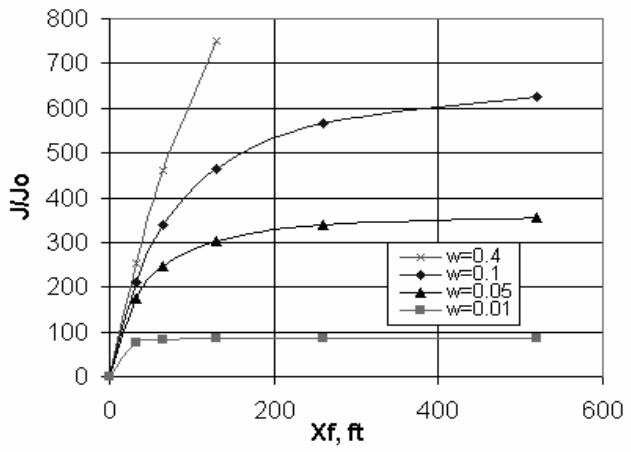

Fig. 20. PI increase after hydraulic fracturing (R_{DO}=60 ft).

Table 3. *Fracture parameters and PIs for all simulations*

Runs	X_f (ft)	w_f (in.)	H_f (ft)	$k_f \times w_f$	WPI4	J/Jo
NO FRAC	0	0	0	0	5	1
FRAC1	32	0.1	100	2275	1050	210
FRAC2	65	0.1	100	2275	1698	339.6
FRAC3	130	0.1	100	2275	2326	465.2
FRAC4	260	0.1	100	2275	2835	567
FRAC5	520	0.1	100	2275	3129	625.8
FRAC6	32	0.4	100	9100	1261	252.2
FRAC7	65	0.4	100	9100	2304	460.8
FRAC8	130	0.4	100	9100	3750	750
FRAC9	32	0.1	50	2275	330	66
FRAC10	65	0.1	50	2275	424	84.8
FRAC11	130	0.1	50	2275	470	94
FRAC12	32	0.01	100	227.5	377	75.4
FRAC13	65	0.01	100	227.5	415	83
FRAC14	130	0.01	100	227.5	428	85.6
FRAC15	260	0.01	100	227.5	434	86.8
FRAC16	520	0.01	100	227.5	434	86.8
FRAC17	32	0.001	100	22.75	79.24	15.848
FRAC18	65	0.001	100	22.75	79.26	15.852
FRAC19	130	0.001	100	22.75	79.27	15.854
FRAC20	32	0.05	100	1137.5	877	175.4
FRAC21	65	0.05	100	1137.5	1241	248.2
FRAC22	130	0.05	100	1137.5	1516	303.2
FRAC23	260	0.05	100	1137.5	1692	338.4
FRAC24	520	0.05	100	1137.5	1771	354.2

in the near-wellbore zone falls below dew point pressure, liquid condensation occurs, which results in a significant decrease in the well productivity (final PI=3.1×10^3 SCFD/STB). The radius of the liquid drop-out region, R_{DO}, during the drawdown periods is estimated to be about 60 ft (R_{DO}=60 ft). The liquid drop-out radius, R_{DO} and, consequently, well impairment predicted by the base model is unreliable (may be overestimated in this case) because of neglecting non-Darcy flow effect in the near-well region, as discussed earlier.

Fracture efficiencies (Fig. 20; Table 3) are compared by well PI derived from Eclipse. The vertical axis in Figure 20 represents PI after fracturing (J) divided by PI before fracturing (Jo), i.e. J/Jo, while the horizontal axis represents the fracture half-length. Each curve corresponds to a different facture width case. It is obvious that hydraulic fracture efficiency starts to flatten as fracture half-length, X_f, extends beyond the liquid drop-out region estimated from pre-fracture simulation (R_{DO}=60 ft). This observation is more obvious at smaller fracture widths.

This simulated hydraulic fracturing study was performed on a well with true (mechanical, damage) skin of 0. The PI increases after hydraulic fracture can exceed the values shown if the well has a damage skin greater than zero (Rae *et al.* 1999). Another factor, which can reduce the well PI values calculated in this section, is the fact that PI values (presented here) were calculated in a transient flow regime. As mentioned before, it was not possible to reach a stabilized pressure (pseudo steady state) regime during the drawdown period. Thus, additional work is suggested to determine which effect is more dominant on the well PI (skin factor versus flow conditions: transient and pseudo steady state).

One conclusion from this study indicates that the PI from a narrow and long hydraulic fracture is smaller than the PI from a short but wide hydraulic fracture (J/Jo is 626 for the first case, 750 for the second case). The terms 'narrow' and 'long' are used for fractures with widths of 0.1″ and a maximum fracture half-length of 520 ft investigated in the study. The terms 'wide' and 'short' are used for fractures with widths of 0.4″ and a half-length of 130 ft. A comparison of these two types of fractures is shown in Figure 21 for a range of fracture half-lengths. Therefore, a hydraulic fracturing procedure should aim to increase fracture width rather than half-length by the application of special techniques, such as tip screen out (TSO).

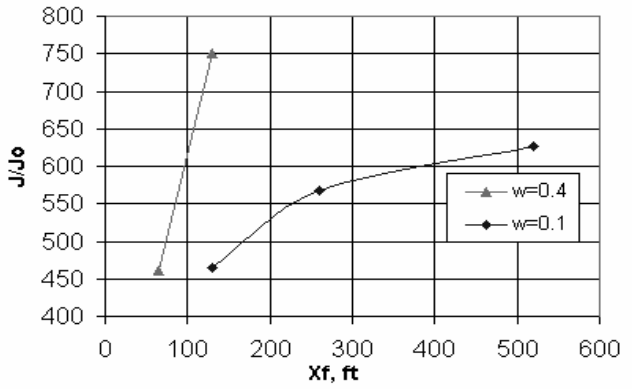

Fig. 21. PI comparison between those fractures derived from models with short/wide and long/narrow fractures.

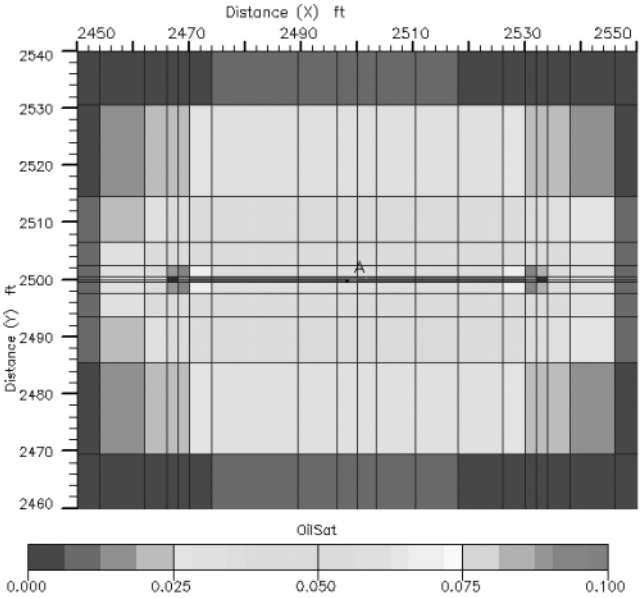

Fig. 22. Liquid saturation around a small fracture at the end of last drawdown (X_f=32 ft, w_f=0.1″).

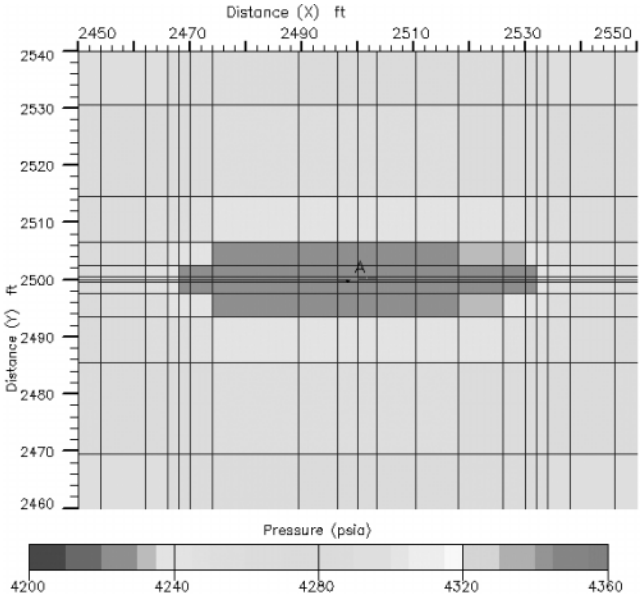

Fig. 23. Pressure profile around a small fracture at the end of last drawdown (X_f=32 ft, w_f=0.1″).

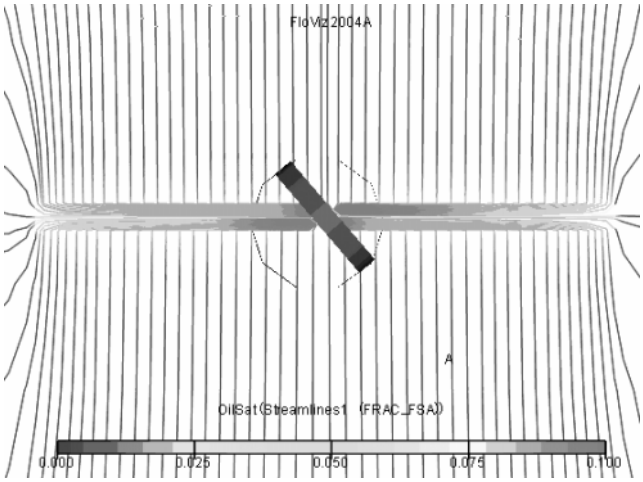

Fig. 24. Linear flow in and to the fracture. Flow convergence at the tip of the fracture can be observed.

PRESSURE AND SATURATION DISTRIBUTION AROUND THE FRACTURE

The hydraulic fracture cases are simulated using the same rate history as that in the non-fracture case (Fig. 19). Figures 22–23 show the liquid saturation and pressure profile around a shorter (X_f=32 ft) hydraulic fracture with the same width (w_f=0.1″). As expected, pressure drawdown around a long fracture is smaller compared with the short fracture case. There is no liquid drop-out during drawdown periods. The saturation profile around the small fracture (Fig. 22) shows that most liquid accumulation occurs at the fracture tips. The same effect was also observed on the saturation profile around X_f=65 ft. It is recommended that additional simulations be performed with different grid sizes in order to determine if this observation is due to grid effect or an actual behaviour due to flow convergence into the fracture.

Additional streamline simulations using FrontSim were performed to study flow profile around a fractured well. Linear flow regimes are observed in the fracture towards the well and from formation to the fracture in the near-well region, as shown in Figure 24. Figure 24 also shows how flow converges into the fracture tips. As flow moves away from the well, it becomes more radial or pseudo-radial (Fig. 25), in which case the fracture behaves as a horizontal well.

The streamline simulation in this case helps in understanding and visualizing flow regimes developed in the reservoir around the fracture and away from it.

CONCLUSIONS

This study has performed some basic multi-phase flow simulations in a fractured gas-condensate reservoir. Hydraulic fractured well productivity evaluation was made through simulation of variable rate well testing. Some very interesting points found during this study are summarized below.

- Well PI impairment due to liquid drop-out in a gas-condensate reservoir will be overestimated if the simulation model ignores the non-Darcy flow effect in the near-well region.
- A hydraulic fracture does not need to be very long to result in a higher PI increase (as long as it passes through the

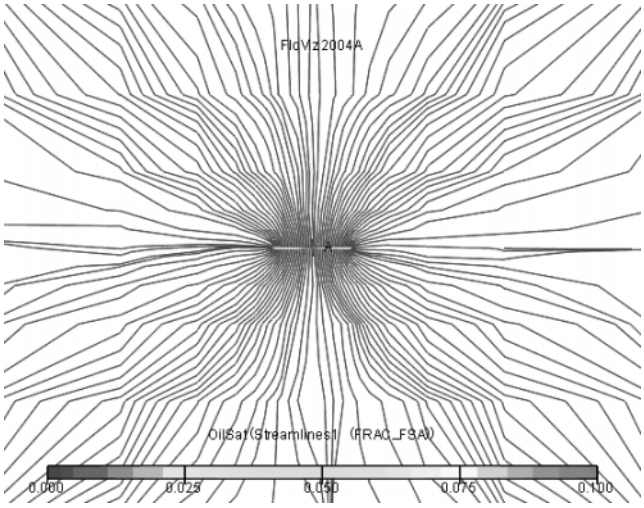

Fig. 25. Pseudo-radial flow away from the well – fracture behaves as a horizontal well.

condensate banking radius, which is usually very close to the well).

- A more important fracture parameter in tight gas-condensate reservoirs is fracture width rather than length. The benefit from increasing fracture half-length diminishes after the length has reached a certain value.
- The study shows that wide/short fractures provide higher PI than narrow/long fractures in a tight gas-condensate reservoir.
- The application of an additional simulation method, such as streamline simulation, can help understanding some engineering concepts easily.

Due to the time limits of the study, some key issues were identified but not fully addressed. These are recommended for future study.

- The study is limited by only one set of fluid data (composition, CGR) and reservoir parameters (k_{abs}, k_{rg}, k_{ro}, k_v/k_h); it is recommended that similar studies are performed using a range of fluid and reservoir datasets, as well as including effects such as non-Darcy flow and dynamic relative permeability.
- Additional work is recommended to determine the time required for the formation of a stable condensate bank, given ranges of reservoir and fluid properties in a tight gas-condensate reservoir.
- The hydraulic fracture simulations showed more liquid accumulation occurs at the tips of a short fracture. Further study is required to determine whether this is due to grid effect or if it is the 'true' case.

Thanks and appreciation to Geoquest RT, Schlumberger for the financial support provided to one of the authors during a MSc summer project. Edinburgh Petroleum Services (EPS), Weatherford and Geoquest RT are also acknowledged for their provision of the software to conduct this study.

APPENDIX A: Nomenclature

CGR, condensate-gas ratio (STB/ $\times 10^6$ SCF)
C_t, total compressibility (psi^{-1})
F_C, fracture conductivity (mD ft)
GOR, gas-oil ratio (MSCF/STB)
H_f, fracture height
k_f, fracture permeability (mD)
k_{in}, inner zone permeability (mD)
k_{out}, outer zone permeability (mD)
k_{abs}, absolute permeability (mD)
k_{effg}, effective permeability to gas phase (mD)
k_{rg}, gas relative permeability
k_{ro}, oil relative permeability
μ, viscosity (cp)
?, porosity (fraction)
P_{bh}, bottom-hole pressure (psi)
P_{dew}, Dew point pressure (psi)
PI, productivity index ($\times 10^3$ SCFD/psi)
P_{net}, effective stress (psi)
P_{ob}, overburden pressure (psi)
P_{pore}, pore pressure (psi)
P_r, reservoir pressure (psi)
ρ_g, gas density (lb/ft^3)
ρ_o, oil density (lb/ft^3)
S_{we}, connate water saturation
S_g, gas saturation
S_o, oil saturation
ν, Poison's ratio
w_f, fracture width (in.)
X_f, fracture half-length (ft)

REFERENCES

Bertram, D.A., Van de Leemput, L.E.C., McDevitt, B.S. & Al Harthy, N.M.A. 1997. *Experience in Gas Condensate Well Test Analysis using Compositional Simulation*. Paper SPE 37994.

Blom S.M.P. & Hagoort, J. 1998. *The Combined Effect of Near-Critical Relative Permeability and Non-Darcy Flow on Well Impairment by Condensate Drop Out*. Paper SPE 51367, SPE REE October.

Carlson, M.R. & Myer, J.W.G. 1995. *The Effects of Retrograde Liquid Condensation on Single Well Productivity Determined vie Compositional Modeling of a Hydraulic Fracture in a Low Permeability Reservoir*. Paper SPE 29561.

Economides, M.J. & Nolte, K.G. 2000. *Reservoir Simulation* 3rd edn. John Wiley & Sons Ltd, Chichester.

Howard, G.C. & Fast, C.D. 1970. *Hydraulic Fracturing*. SPE Monograph, **2**.

Jones, J.R. & Raghavan, R. 1988. *Interpretation of Flowing Well Response in Gas Condensate Wells*. Paper SPE 14204.

Rae, P., Martin, A.N. & Sinanan, B. 1999. *Skin Bypass Fracs: Proof That Size Is Not Important*. Paper SPE 56473.

Saleh, Amer M. 1992. *Well Test and Production Prediction of Gas Condensate Reservoirs*. PhD thesis. Petroleum Engineering Department, Heriot-Watt University, Edinburgh.

Settari, A., Bachman, R.C., Hovem, K. & Paulsen, S.G. 1996. *Productivity of Fractured Gas Condensate Wells – A Case Study of the Smorbukk Field*. Paper SPE 35604.

Towler, B.F. 1999. Fundamental Principles of Reservoir Engineering. *SPE Textbook Series*, 8.

Yadavalli, S.K. & Jones, J.R. 1996. *Interpretation of Pressure Transient Data From Hydraulically Fractured Gas Condensate Wells*. Paper SPE 36556.

Received 12 November 2004; revised typescript accepted 28 April 2006.